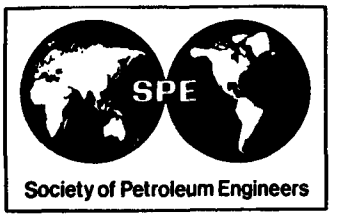

SPE 24880

A Pore-Level Scenario for the Development of Mixed Wettability in Oil Reservoirs

C.J. Radke,* A.R. Kovscek,* and H. Wong, U. of California

*SPE Members

Σ

This paper was prepared for presentation at the 67th Annual Technical Conference and Exhibition of the Society of Petroleum Engineers held in Washington, DC, October 4–7, 1992.

Abstract

Understanding the role of thin films in porous media is vital if wettability is to be elucidated at the pore level. The type and thickness of films coating pore walls determines reservoir wettability and whether or not reservoir rock can be altered from its initial state of wettability. Pore shape, especially pore wall curvature, is an important factor in determining wetting film thickness. Yet, pore shape and the physics of thin wetting films are generally neglected in models of flow in porous rocks. This paper incorporates thin wetting film forces into a collection of capillary tubes model to describe the geological development of so-called mixed-wettability in reservoir rock. Our model emphasizes the remarkable role of thin films.

New pore-level fluid configurations arise that are quite unexpected. For example, efficient water displacement of oil (i.e., low residual oil saturation) characteristic of mixed-wettability porous media comes about due to interconnected oil lenses or rivulets which bridge the walls adjacent to a pore corner.

Predicted residual oil saturations are found to be approximately 35 percent less in mixed-wet rock when compared to completely water-wet rock. Calculated capillary pressure curves mimic those of mixed-wet porous media in the primary drainage, imbibition, and secondary drainage modes. Amott-Harvey indices range from -0.18 to 0.36 also in good agreement with experimental values[1,2].

References and illustrations at end of paper

Introduction

The wettability of reservoir rock is a critical factor in determining the displacement effectiveness and ultimate oil recovery by drive fluids, such as water. Since the most wetting fluid tends to occupy the smallest and, hence, most hydrodynamically resistive pore channels while the least wetting fluid distributes to the largest and least resistive pore channels, wettability is a prime factor controlling multiphase flow and phase trapping. Therefore, understanding how wettability is established at the pore level is crucial if predictive flow models are to be developed.

Wettability in porous media is generally classified as either homogeneous or heterogeneous. For the homogeneous case the entire rock surface has a uniform molecular affinity for either water or oil. Conversely, heterogeneous wettability indicates distinct surface regions that exhibit different affinities for oil or water.

Three broad classifications of homogeneous wetting exist: strongly water-wet, strongly oil-wet, and intermediate wet. If smooth representative rock surfaces can be prepared, then contact angles for water-wet surfaces, measured through the water phase, are near zero. Whereas, for oil-wet surfaces they are near 180°. In the case of intermediate-wetting, the rock has neither a strong affinity for water nor oil, and contact angles range roughly from 45° to 135°[3].

Two types of heterogeneous wettability are generally recognized. Mixed-wettability refers to distinct and separate water-wet and oil-wet surfaces which coexist and span a porous medium. Dalmation, also speckled or spotted, wettability refers to continuous water-wet surfaces enclosing

macroscopic regions of discontinuous oil-wet surfaces or vice-versa [4].

For many years, it was common petroleum-engineering practice to assume that oil reservoirs are strongly water-wet. Because most reservoir rock is highly siliceous and because oil reservoirs evolve by oil migrating into initially brine-occupied pore space, it was thought that the rock surface maintains a strong affinity for water even in the presence of oil[5]. In 1973, however, Salathiel[6] established that reservoirs with mixed-wettability display low residual oil (i.e., oil trapped as isolated globules) and consequently high displacement efficiency, as gauged by the ratio of oil recovered after waterflooding to the original oil in place. More recently, Fassi-Fihri et al[7] used cryo-scanning electron microscopy to confirm that wettability is heterogeneous on the pore scale in actual reservoir media and that mineralogy greatly affects the type of wettability.

The purpose of this paper is to develop a pore-level picture of how mixed-wettability might form and evolve in reservoir rock initially filled with brine. Before embarking on this task we briefly explore the relationship between thin films and wettability.

Thin Films and Wettability

A succinct description of mixed-wettability follows when the effects of thin films which coat and adhere to solid surfaces are considered. Thin-film forces in fact control wettability.

Figure 1 displays a schematic diagram of an apparatus used to quantify thin-film forces in liquid films adjacent to a solid surface[8]. An annular porous disk, which allows flow of wetting fluid, is sealed against a solid substrate. A nonwetting fluid meniscus enters from below the solid substrate disk assembly. Far away from the solid substrate, the meniscus is hemispherical. When the central portion of the meniscus is pressed against the wall, a thin film forms. As the pressure of the nonwetting fluid rises compared to that in the wetting fluid, the film thins and the meniscus or Plateau border recedes into the corner. An experiment proceeds by applying a capillary pressure difference (i.e., $P_c = P_{nw} - P_w$) across the Plateau-border meniscus and measuring the resulting thickness of the film by interferometry or ellipsometry.

At equilibrium, the pressure of the wetting fluid in the thin film and the Plateau border are identical. The film is flat, yet the capillary pressure is nonzero. Consequently, the standard Young-Laplace equation of capillarity does not describe the thin film portion of Fig. 1. Rather, thin-film forces must be incorporated into the Young-Laplace equation by adding a term, $\Pi(h)$, referred to as disjoining pressure[9-12]:

$$P_c = \sigma\left(\frac{1}{r_1}+\frac{1}{r_2}\right) + \Pi(h) \cdot \qquad (1)$$

In the augmented Young-Laplace equation, σ refers to the bulk interfacial tension between the wetting and nonwetting phases for an interface with principal radii of curvature r_1 and r_2.

Disjoining pressure is a function of film thickness, h. If disjoining pressure is positive, the two interfaces are repelled, whereas if disjoining pressure is negative the two interfaces are attracted. When films are thin (e.g., 100 nm), the disjoining pressure is significant compared to the other terms in Eqn. (1). For the flat film in Fig. 1, the curvature is zero so that at equilibrium $P_c = \Pi(h)$. Equation 1 may be cast in dimensionless form by a characteristic force, σ, and a characteristic dimension, a_m. Representative values of σ and a_m are 50 mN/m and 150 μm respectively. With this scaling, the first term on the right side of Eqn. (1) varies from approximately 1/3 to 10 whereas a disjoining pressure of 500 Pa makes the second term of order 1.

A schematic disjoining pressure isotherm is drawn in Fig. 2. For certain values of disjoining pressure, for example Π_1, there are three possible equilibrium film thicknesses. The outermost films have thicknesses of order 10 to 100 nm. The central portion of the Π versus h curve (i.e., where $d\Pi/dh$ is positive) is an unstable region[13]. A film in this thickness region spontaneously thickens or thins to a new stable configuration. The innermost films are quite thin, possibly on the order of one or several monolayers of solvent molecules. The effective range of the disjoining pressure is denoted by h_p.

Many factors contribute to the shape of a disjoining pressure isotherm. Three major force components are electrostatic interactions, van der Waals interactions, and hydration forces[14]. The first, electrostatic forces, originate from the overlap of ionic clouds known as electrical double layers present at each interface. For symmetric charged films, these are repulsive stabilizing forces[15]. Melrose[14] and Hall[17] give thorough discussions of double-layer repulsive forces and their effects on film stability. Dispersive van der Waals forces are usually attractive and destabilize thin-aqueous films[14]. Lastly, strong repulsive hydration forces are important at film thicknesses approaching molecular dimensions[17].

Clearly, the mineral content of pore walls has a large effect on thin-film interaction forces. For example, when a drop of crude oil is contacted with a brine-covered surface, crude oil adheres more readily (i.e., thick aqueous films break more easily) on calcite than quartz[18]. Because calcite has a more positive surface charge, under identical conditions there is lesser stabilizing repulsive action from the electrostatic overlap forces.

Oil-drop adhesion tests provide a simple approach to characterize the wetting behavior of crude oils against solid surfaces[1,19,20]. When adhesion occurs, it is found that the solid/oil/water boundary is fixed or "pinned" at the three-phase contact line[18]. Accordingly, the contact line of a retracting oil drop does not recede along the solid substrate. In subsequent sections, the importance of contact-angle pinning in mixed-wettability systems will become evident.

Thin-film forces determine the contact angle. Direct integration of the augmented Young-Laplace equation yields the following relationship between contact angle, θ, and disjoining pressure[21]

$$\cos\theta - 1 = \frac{1}{\sigma}\left[\int_h^{h_p} \Pi d\xi - (h_p - h)\Pi(h)\right]. \quad (2)$$

In Eqn. (2), h is the equilibrium film thickness of interest. Implicit in Eqn. (2) is the constraint that $h_p/a_m << 1$.

Integration over the positive purely repulsive portions of Fig. 2 (i.e., the thick outer films) results in zero contact angle. Conversely, nonzero contact angles up to 90° are possible when Eqn. (2) is integrated[21] over the attractive negative portions of Fig. 2. The above equation is derived for a meniscus attached to a flat solid surface. Nevertheless, it still applies for solid curved surfaces as long as the film thickness is much smaller than the radius of curvature of the surface.

Consider now films on significantly curved surfaces. Figure 3 displays one such surface: two spherical solid beads with diameters d_1 and d_2 covered with a layer of wetting fluid. The curvature of the films is nonzero and the curvature term on the right side of Eqn. (1) now contributes. If the wetting films are convex, as in Fig. 3, the curvature of the interface is negative.

Assume now that the films in Fig. 3 are under an imposed capillary pressure and that the films are thin enough so that the curvature of the film far away from the bead contact is roughly that of the bead (i.e., h/d << 1). In this situation, the smaller the bead diameter the more negative is the film curvature. Rearranging Eqn. (1) and invoking the geometry of Fig. 3 we find that

$$\Pi(h_i) = P_c + \frac{4\sigma}{d_i}. \quad (3)$$

Thus, to maintain equilibrium with a fixed capillary pressure, the film disjoining pressure must rise as the diameter, d_i, of a bead decreases. Accordingly, the film coating the smaller bead is thinner than that coating the larger bead. The second term on the right side of Eqn. (3) contributes 2000 Pa when d_i is 100 μm and σ is 50 mN/m.

According to Fig. 2, film thickness decreases monotonically with increased capillary pressure until the local maximum in disjoining pressure, Π^{max}, is reached. This corresponds to a critical capillary pressure, P_c^*, for thin film rupture. When the capillary pressure exceeds P_c^*, the thick outer film sheets away and only a molecularly adsorbed film resides next to the surface. Because the disjoining pressure is largest in the film coating the smallest bead, that film becomes unstable first and consequently has the smallest P_c^*. Inserting Π^{max} into Eqn. (3) gives P_c^* for any bead diameter. Equation 2 teaches that exceeding the critical capillary pressure also signals a transition in the contact angle. Our discussion so far is quite general and applies to oil films between a solid and brine as well as aqueous films between a solid and oil. Next, we discuss one manner in which a water-wet surface transforms into an oil-wet surface.

When a thick aqueous wetting film collapses into a molecularly thin one, surface active components from asphaltic oil can, in some instances, adsorb irreversibly onto the surface. Asphaltenes (i.e., high molecular weight aggregates insoluble in light normal alkanes but soluble in benzene and pyridine) occur in relatively large quantities in many crude oils. Apparently, asphaltenes are colloidal polydispersions comprised of flat, disklike aggregates[22]. They are usually coated with lower molecular weight resins[23]. Resins adsorbed to the asphaltene surfaces apparently stabilize the asphaltene colloidal dispersions.

Clementz[24,25] demonstrated that the heavy ends fraction of crude oil (i.e., asphaltenes) adsorbs strongly to clay materials at low water content. Also, Dubey and Waxman[22] showed that asphaltenes adsorb quite readily to clay materials in the absence of both brine and resins. The asphaltene aggregates apparently adsorb with their disk faces against the planar faces of the clay. Asphaltene adsorption appears irreversible for all practical purposes [1,22,26]. Strong solvents and extensive cleaning procedures are necessary to desorb asphaltenes and resins. The key factor in asphaltene adsorption appears to be direct access of the asphaltic components of the oil to the rock surface without an intervening thick layer of water in which they are highly insoluble. Thus when the critical capillary pressure is exceeded, asphaltenes may adsorb because only a molecular aqueous film protects the solid surface.

In practice, surfaces within porous reservoir rock are curved and rough. Hence, it is difficult to measure contact angles and to determine the extent of connectivity of water and oil-wetting surfaces. Fortunately, capillary pressure as a function of water saturation exhibits characteristic shapes for different types of wettability in porous media[4,18].

Description of the geological evolution of mixed-wettability proceeds in a manner similar to the generation of capillary pressure curves. Pore-level events are followed through the cycle of primary drainage, spontaneous imbibition, forced imbibition, and secondary drainage. Asphaltene adsorption onto solid surfaces is allowed if thick protective water films break. Theoretical capillary pressure curves are calculated and the extent of oil-wettability gauged via Amott-Harvey indices.

Theory

Initially, reservoir rock is saturated with brine (brine and water are used interchangeably) and strongly water-wetting. Reservoir rock which is unaltered from its original state is referred to as pristine. Actual pores in reservoir media are lined by

nooks or axial grooves[13]. Accordingly, the porous medium is modeled as a collection of star-shaped translationally invariant pores, as illustrated in Fig. 4. The star shape is chosen because it is nonaxisymmetric, cornered, and resembles the open area between 4 rods or 4 sand grains in cross section when they are in contact. The radius of the largest circle which can be inscribed in a pore is denoted as a. We adopt such a simple model of a porous medium to emphasize the remarkable role of thin films on wettability. Because reservoir-scale flow rates are low, all continuous phases are assumed in capillary equilibrium. Gravity and end effects are not considered. Capillary pressure is consistently defined as the oil-phase pressure minus the aqueous-phase pressure.

Figure 5 shows on a semi-logarithmic scale the size distribution of star-shaped pores employed here. The distribution is nondimensionalized by the mean of the distribution, a_m, taken here as 150 μm. This particular distribution approximates roughly that found by Wardlaw et al[27] for pores in a Berea sandstone. In addition to pore bodies, the chosen distribution also contains a significant number of pores which are exceptionally small. These small pores represent pore throats and micropores. The frequency scale indicates the actual number of pores of that size used in the calculations to follow.

Single Pore Events

First, consider a single brine-filled pore of size a that is highly water-wet. Brine cannot drain from this tube until the capillary entry pressure, P_c^e, is exceeded. For star-shaped pores with a 0° contact angle, the capillary entry pressure[28] is given by

$$\frac{aP_c^e}{\sigma} = 1.86 \cdot \qquad (4)$$

Oil then enters the tube with a constant meniscus curvature displacing brine from the central portion of the tube leaving brine only in the corners. This oil-invasion process is illustrated in Fig. 6. Light shading represents brine while dark shading represents oil. Thick aqueous films lie between the solid pore walls and the oil. Their thickness is determined by the capillary pressure and the form of the disjoining pressure isotherm (c.f. Fig. 2). The configuration of the brine-filled corners far behind the invading meniscus is that of constant curvature circular arcs.

The curvature of the so-called arc menisci [29] does not change until the invading meniscus empties the entire middle portion of the tube. After the central portion of the tube fills with oil, the arc menisci increase their curvature in response to higher imposed capillary pressures and move toward the cusp. Thus, as the capillary pressure climbs, more oil enters the tube, the aqueous films coating pore walls thin, and the disjoining pressure climbs.

When the critical capillary pressure, P_c^*, for this sized pore is attained, the thick films become unstable and spontaneously thin to molecularly adsorbed films. Since h/a << 1, the thick films coating the walls of star-shaped pores have approximately the same curvature as the pore walls. Consequently, the critical capillary pressure for thick wetting-film collapse is

$$P_c^* = \Pi^{max} - (\sqrt{2} - 1)/a \, . \qquad (5)$$

The second term on the right incorporates the curvature of the film adhering to the pore wall. It is negative (because the pore wall is convex) causing P_c^* to be less than Π^{max}, the local maximum in disjoining pressure (c.f. Fig. 2). For smaller pore sizes the critical capillary is smaller and vice versa.

In accordance with Eqn. (2), the ultrathin molecular films produced for $P_c > P_c^*$ do not result in the same contact angle as that for the initial thick wetting films. Disjoining pressure isotherms have not been measured for solid/water/oil systems of interest. Accordingly, we approximate contact angles for the molecular aqueous films as 20° rather than calculate specific contact angles for each film thickness. The contact angle is 0° for the thick films since they lie on the purely repulsive portion of the disjoining pressure curve. The known phase configurations now lead directly to the aqueous phase saturation, $S_w = A_w/A_t$, where A_w is the cross-sectional area of the pore occupied by water and A_t is the cross-sectional area of the pore.

The capillary pressure versus aqueous phase saturation curve for the entire size distribution of Fig.5 is calculated in a fashion similar to that described above: interfacial curvature is incremented by imposing new capillary pressures, pore-level reconfiguration of fluids is assessed, and the saturation is calculated from a knowledge of interfacial curvature and fluid configuration. Numerical and geometrical details of the calculation are available elsewhere [30]. Once garnered, the P_c versus S_w curve is available for comparison to typical experimental data.

Pristine Drainage

Pristine drainage occurs between the points labelled A through C on the capillary pressure curve shown in Fig. 7. No oil enters the porous medium until point A where the capillary entry pressure is exceeded for the largest sized pore. Each particular pore size has a unique entry pressure determined by Eqn. (4). As the capillary pressure climbs, oil flows into the porous medium, more capillaries are entered, the menisci in the oil-occupied pores are forced farther into the corners of the pores, and water films coating the walls of the capillaries become thinner. The curve displayed in Fig. 7 is not smooth because a discrete rather than smooth distribution of pore sizes is employed (c.f. Fig. 5).

Each sized pore, following Eqn. (5), has a unique critical capillary pressure for film stability. Films are thinnest along pore walls with the most negative curvature (i.e., those pores with the smallest radii of curvature). Thick protective water films coating pore walls correspondingly rupture or sheet away, for

instance near point B on Fig. 7, in the smallest oil occupied pores. The drainage and film-breakage processes continue to P_c^{max} the highest imposed capillary pressure (point C on Fig. 7). Water saturation at this point is defined as connate saturation, S_{wc}.

Consistent with Salathiel's original observations, large applied capillary pressures, such as P_c^{max} in Fig. 7, correspond to low connate water saturation[6]. It is possible to reduce water saturation further by exceeding P_c^{max}, because both phases maintain continuity throughout the pore structure. That is, no water is trapped at connate saturation in Fig. 7.

After water drainage to P_c^{max} the following fluid distributions are found. The smallest pores which have not undergone oil entry are completely water filled, the intermediate-sized pores exhibit molecular films with contact angles of approximately 20° and water-filled corners, and the largest pores exhibit thick protective films with contact angles of 0° and water-filled corners.

Asphaltene Adsorption

Oil reservoirs remain at connate water and P_c^{max} for geological periods of time. We assert that asphaltenes adsorb along the pore walls of the oil-occupied intermediate-sized pores where thick protective water films are broken. The location along pore walls where asphaltenes adsorb is displayed schematically in Fig. 8 as a white region recessed from the pore wall.

No asphaltene adsorption occurs within the largest pores because thick protective water films coat pore surfaces. Because asphaltenes are insoluble in water, it is apparently not possible for them to dissolve in and transport across the thick water films to contact the pore walls. However, the resin-coated asphaltene aggregates are much larger than the molecular dimensions of water. Hence, they can, over time, span the molecular layers of water coating intermediate-sized pores causing some water molecules to desorb and directly contact the rock surface adsorbing irreversibly. Salathiel[6] was able to observe such asphaltene adsorption on sandstones within hours. It is not clear whether the resins coating the asphaltene colloids or the asphaltene aggregates themselves actually bind to the surface in the presence of molecular water films.

Figure 8 also illustrates that two distinct regions of wettability exist along the walls of intermediate-sized pores. The corners of the pore retain bulk water preventing asphaltene adsorption and thus preserve their water-wettability. Away from pore corners the highly hydrophobic adsorbed asphaltenes make that portion of the pore wall oil-wet. We designate this type of pore as mixed-oil-wet.

A step change in wettability exists at the contact line between the asphaltene-coated portion of the pore wall and the water-filled corner. This contact line is pinned at the position it achieved at P_c^{max} and does not move in response to changes in capillary pressure. Rather, changes in capillary pressure are accommodated by changes in the angle of the pinned, three-phase contact line and the local interfacial curvature. The pinned contact angle is free to assume values between 20° and 180°.

After asphaltene adsorption at P_c^{max}, the smallest pores which were never entered by oil are completely brine filled, the intermediate-sized pores, which exceeded their critical capillary pressure for thin film stability, P_c^*, have asphaltenes adsorbed on the rock surface and hence are mixed-oil-wet with the contact line between the oil and water-wet regions pinned. The largest pores, which did not exceed their corresponding P_c^*, remain water wet.

Spontaneous Imbibition

Upon reduction of the imposed capillary pressure, water imbibes spontaneously due to capillary suction. If imbibition is controlled, equilibrium capillary pressures are measured. Spontaneous imbibition occurs between the points labelled C through E on Fig. 7, and all pores refill with water. In the largest oil-occupied, water-wet pores, the corner menisci follow the reverse of their pristine drainage course in response to the decreasing capillary pressure. As the capillary pressure falls, the menisci move farther away from the corner at zero contact angle. This continues until the menisci touch to form an inscribed circle (see Fig. 9a). The inscribed circle configuration is unstable[31] in that any infinitesimal disturbance in the streamwise direction will grow. As described by Roof[32], the oil snaps off in order to achieve a minimum energy configuration.

Morrow and Mason[29] argue that for perfectly wetting triangular pores, the snapped-off oil exhibits curvatures corresponding to the entry curvature. We adopt the same reasoning here and demand that the curvature of the snapped-off oil drop be that given by Eqn. (4). Thus, snapped-off oil is distributed along the length of the water-wet pores as isolated cylinders of oil resembling sausages with hemispherical end caps and curvatures corresponding to the appropriate entry curvature. The length of the oil cylinders is determined by the long wavelength disturbances which cause breakup of the oil column, roughly $2\pi a$ [13].

After snap-off, the isolated oil sausages are no longer connected with the continuous oil fraction and are, therefore, no longer under the influence of the applied capillary pressure. In our equilibrium scenario, there is no facility to displace this discontinuous oil. Even if small axial pressure gradients are imposed the disconnected oil eventually encounters a pore constriction and traps. Therefore snapped-off oil is termed here as residual oil. Figure 7 labels the region D where oil snap-off and trapping occurs.

In the intermediate-sized, mixed-oil-wet pores spontaneous imbibition is a less dramatic process (Fig. 9b). Recall that the three-phase contact line in mixed-oil-wet systems is pinned at the location it attains at P_c^{max}. When brine imbibes into these pores, the curvature of the pinned oil/water interface simply decreases until it reaches zero. Examination of Fig. 9b reveals that small changes in the brine

saturation of mixed-oil-wet pores cause large changes in interfacial curvature and thus in capillary pressure. This explains the near step change in P_c near point E of Fig. 9. In the vicinity of point E, all of the water-wet pores contain residual oil so that only the mixed-oil-wet pores undergo saturation changes.

At zero imposed capillary pressure the smallest pores which were not entered by oil are completely brine filled, the intermediate-sized, mixed-oil-wet pores contain continuous oil in the center of the pores and continuous brine in the corners of the pores with an interfacial curvature of zero, and the largest water-wet pores contain stationary, discontinuous residual oil surrounded by continuous brine.

Forced Imbibition

Further imbibition occurs along points E through G of Fig. 7 when water is forced into the rock. Changes occur only in the mixed-oil-wet pores because, as above, the smallest pores are completely brine filled and the largest water-wet pores are filled with trapped oil. Water-phase pressure now exceeds oil-phase pressure. Hence, negative capillary pressures arise.

Because the fraction of water-wet surfaces in the mixed-oil-wet pores is quite small, the pore appears completely oil-wet (i.e., a contact angle of 180° measured through the water phase) to the water-invasion process. Thus, water invasion is directly analogous to oil entry for completely water-wet pores (i.e., a contact angle of zero). Accordingly, the entry curvature is given by

$$\frac{aP_c^e}{\sigma} = -1.86 , \qquad (6)$$

where the negative sign arises because of the 180° contact angle (c.f., Eqn. (4)). Water imbibes into progressively smaller mixed-oil-wet pores as the capillary pressure becomes more negative (e.g., point F on Fig. 7).

Figure 10 displays the oil and water configurations in a mixed-oil-wet pore just after water invasion. A thick lens or rivulet of oil bridges the corner of the pore separating brine in the pore center from that in the pore corner. This bridging oil-lens configuration is readily argued to be stable[31]. An oil film coats the central portion of the pore wall. The original three-phase contact line nearest the corner remains pinned while the newly created meniscus establishes an equilibrium contact angle against the pore wall.

Since asphaltene adsorption is virtually irreversible[1,22,26], we postulate that all thicknesses of oil films deposited on asphaltene-coated surfaces are stable. It follows that the oil-film disjoining pressure is purely repulsive. Thus, the solid surface is completely wetted by oil, and the newly created meniscus makes a contact angle of 180° measured through the water phase. If measured through the through the oil phase, the contact angle is zero following a monotonic repulsive disjoining pressure isotherm and Eqn. (2). More structure to the oil-film disjoining pressure isotherm is possible[17], but leads in our model to no significant differences in overall pore-occupancy configurations.

Oil contained in the lens of Fig. 10 is translationally continuous. Consequently, all of the oil drains, although slowly, from the lens as the capillary pressure becomes more negative. When the lenses are nearly empty of oil, the two water/oil interfaces composing the lens meet. The imposed negative capillary pressures are sufficient to cause lenses in all mixed-oil-wet pores to touch. The lenses do not meet at the same imposed capillary pressure because pore-wall curvature varies among pores.

Two possibilities exist for the behavior of the oil lenses when the water/oil interfaces touch. In case 1 the lens is unstable and breaks. The small amount of oil contained in the lens when it breaks flows via the continuous oil-wet surfaces to surrounding pores and is distributed equally among the remaining oil lenses. Hence, the curvature of the remaining lenses decreases slightly. In case 2 a film, like that in a stable water-in-oil (W/O) emulsion, is created which bridges the pore corners. A repulsive, stabilizing disjoining pressure in the thin water/oil/water film is required for case 2. We assume here that the W/O emulsion films are stable within the range of applied capillary pressures. If the W/O emulsion films are not stable over the range of capillary pressures applied, case 1 is recovered.

Regardless of which picture is adopted, the oil saturation of the system decreases to S_{or}, the residual oil saturation. At P_c^{min}, point G on Fig. 7, the smallest pores which were not entered by oil during primary drainage remain completely brine filled, the intermediate-sized, mixed-oil-wet pores are completely filled with water except for a small oil fraction which exists as either thin oil films along the solid surface of the pores or as W/O emulsion films which span each corner of the pore, and the largest pores which remained entirely water-wet (i.e., exhibit no asphaltene adsorption) contain snapped-off oil which gives rise to S_{or}.

Secondary Drainage

During secondary drainage of water, the calculated capillary pressure curves differ for cases 1 and 2. Secondary drainage for unstable lenses occurs between points G through K on Fig. 7, whereas secondary drainage for the stable emulsion films occurs between points G and M through P on Fig. 11.

In the case of unstable lenses, beginning at the minimum imposed capillary pressure, the oil films lining the walls of mixed-oil-wet pores begin to thicken following Eqn. (1). The oil must reside as thin films until the capillary pressure exceeds the curvature of the wall (i.e., $P_c \geq (\sqrt{2}-1)/a$; point H on Fig. 7). Figure 12 shows the pertinent fluid configurations once the capillary pressure exceeds the curvature imposed by the wall.

With increasing positive capillary pressure, oil continues to invade along the pore walls of Fig. 12. Pinning is still demanded at the step change in

wettability along the pore surface. Once the oil interfaces touch an unstable fluid configuration arises. The brine in the very center of the pore rearranges into cylindrical droplets with hemispherical endcaps which span pore cross-sections. In cross-section, these fluid configurations are very similar to those displayed in Fig. 10 for forced imbibition except that the outermost pinned oil/water interfaces bow toward the pore corners. Oil maintains continuity along the length of the pore, but the brine in the center of the pore is no longer continuous. Individual discontinuous brine droplets are separated axially by thick oil bridges perpendicular to pore walls connected to the oil lenses running the length of the pore. This discontinuous brine is the direct analogue to discontinuous trapped oil and is the referred to as irreducible water. The label I on Fig. 7 highlights the region where trapped irreducible water is created with saturation S_{wirr}. Note that in strongly water-wet porous media there is no irreducible water. Connate water is continuous; S_{wc} simply decreases as P_c^{max} rises.

During water drainage from the mixed-oil-wet pores, oil also enters the large water-wet pores at the appropriate entry pressure as it did during pristine drainage (see point J on Fig. 7). When oil enters the water-wet pores it reconnects with the residual oil originally trapped in those pores. Oil filling continues until P_c^{max} is reattained at point K Fig. 7.

In the case of stable W/O emulsion films (i.e., case 2), oil refills the thin oil films bridging the corners of the pore beginning at P_c^{min}, as illustrated in Fig.13. The free oil meniscus (i.e., the inner most one which is unpinned) grows at 0° contact angle while the water/oil interface remains pinned at the contact line of the step change in wettability. Once the unstable inscribed circle configuration is attained (see Fig. 13), snap-off ensues and the water disconnects giving rise to irreducible trapped water. The region where irreducible water is created is marked as M on Fig. 11. The shape of the isolated cylinders of irreducible water is quite identical to that for case 1. The only difference is that the isolated water cylinders are separated axially by smaller oil bridges than in case 1.

The applied capillary pressure now rises quite rapidly with little change in saturation in the region around the point N on Fig. 11. Water is trapped in all of the mixed-oil-wet pores and the capillary pressure is not above that necessary for oil to enter any of the water-wet pores. The only saturation change in response to capillary pressure increases occurs in the corners of the mixed-oil-wet pores at the pinned contact line, much as it did at point E on Fig. 7 during spontaneous imbibition.

With capillary pressures now positive, oil enters the water-wet pores, for instance at point O on Fig. 13, and reconnects with the residual oil originally trapped in those pores. Again the capillary pressure increases to P_c^{max}, point P on Fig. 13. In both cases 1 and 2, there are no molecularly thin water films because P_c^* has not been exceeded for any of the remaining water-wet pores.

Once P_c^{max} is reattained the smallest pores never entered by oil are completely brine filled and water-wet. The intermediate mixed-oil-wet pores contain continuous brine in the corners of the pore, continuous oil lenses, and disconnected, irreducible brine in the center of the pores. The largest pores contain continuous oil in the center of the pore and continuous brine in the corners connected to thick continuous water films along the pore walls. If W/O emulsion films do not form (i.e., unstable lenses), irreducible brine is formed while the capillary pressure is positive during secondary drainage. If W/O emulsion films are stable within the range of applied capillary pressure, then irreducible brine is formed while capillary pressures are negative. Thus, both cases result in similar phase configurations at P_c^{max} of secondary drainage.

Results

Capillary Pressure Curves

The above collection of pore-level events leads directly to the theoretical capillary pressure versus aqueous phase saturation curves in Figs. 7 and 11 that are characteristic of mixed wettability[18,33]. Figures 7 and 11 show that, consistent with Salathiel's observations, connate and irreducible water saturations are not equal. This is a result of the wettability alteration which occurs at P_c^{max} during primary drainage. Oil migrates into a reservoir when it is water-wet. Thus, no brine is trapped and the connate or initial water saturation is much less than the irreducible water attained after oilflooding a previously waterflooded reservoir. The pore-level events which occur along the path to P_c^{max} the second time are for a mixed-wet porous medium. Although the same capillary pressures are imposed, the endpoint saturations are quite different. When a second loop from P_c^{max} to P_c^{min} and back to P_c^{max} is made, saturations at P_c^{max} are the same and a scanning hysteresis loop results.

The final saturations after secondary drainage of water for cases 1 and 2 (points K on Fig. 7 and P on Fig. 11) are not equal because the water configurations are different prior to the snap-off process. These configurations, shown in Figs. 12 and 13, determine irreducible water. In light of the pore-level scenario presented here, we find that significant amounts of brine are trapped in mixed-oil-wet pores.

In the next section we turn our attention to Amott-Harvey indices[18,34] and residual oil saturations calculated from the capillary pressure curves of Figs. 7 and 11. We use Amott-Harvey indices to compare further our theoretical results with those commonly obtained experimentally for mixed-wettability porous media.

Porous Medium Wettability

Table 1 presents Amott-Harvey indices, I_{ow}, and residual oil saturation for both of the mixed-wet cases and for a water-wet case (i.e., case 3) ascertained from the theoretical capillary pressure curves. Case

3, the water-wet example, has a nondimensional disjoining pressure maximum ($a_m\Pi^{max}/\sigma$), for aqueous films coating solid surfaces, 10 times larger than the mixed-wettability cases. This ensures that none of the thick water films coating pore walls rupture and become molecularly thin. Asphaltene adsorption is thereby prohibited. Consequently, this case has an I_{ow} of 1 as expected for strongly water-wetting rock. The Amott-Harvey index for the unstable lenses (case 1) is greater than for the stable W/O emulsion film (case 2). Case 2 undergoes significant saturation change during secondary drainage while the capillary pressure is negative, whereas case 1 does not.

The unstable lenses and the stable W/O emulsion film cases exhibit identical residual oil saturations because in each case an identical amount of oil is contained in lenses such as those shown in Fig. 10. Recovery of oil from these lenses is complete. Pore-level events only begin to differ after P_c^{min} and S_{or} are attained.

Relative to the water-wet case, residual oil saturation for the mixed-wet cases is much reduced. This is consistent with experimental observations[2,6]. However, the magnitude of S_{or} obtained experimentally is much lower than predicted here. Our scenario over estimates residual oil primarily because pores are not explicitly interconnected. In actual porous media, the connectivity or topology of the pore space strongly influences the displacement and entrapment of oil[35]. Likewise, irreducible water saturation is larger than that found experimentally also because pore space is not multiply connected. As stated earlier, the issue of multiple connections among pores is not considered here so that the role of thin-wetting films and pore shape may be elucidated.

Salathiel[6] originally attributed extended oil recovery from mixed-wettability rocks to thin continuous oil films along the rock surface which allow almost indefinite oil displacement. In the scenario proposed here, we predict that most recoverable remaining oil occurs as lenses or rivulets which span the corners of mixed-oil-wet pores (c.f., Fig. 10). The oil films coating the oil-wet fraction of the pore walls allow surface drainage of oil, but the oil volumes they contribute is much less than that associated with lens drainage.

Discussion

The above model of mixed-wettability has five important parameters which can be altered: maximum imposed capillary pressure, minimum imposed capillary pressure, disjoining pressure maximum, pore shape, and pore-size distribution. We consider briefly each in turn.

As the maximum imposed capillary pressure is increased, more thick protective water films spontaneously break to molecular films during pristine drainage. A larger fraction of the rock surface is then coated with asphaltenes and becomes oil wet. This effect is consistent with Salathiel's findings. As he decreased connate water saturation and correspondingly increased the imposed capillary pressure, his core samples displayed increased oil-wet behavior. More recently Jadhunandan and Morrow[2] showed experimentally that a porous medium changed from fairly strongly water-wet to mixed-wet by reducing connate or initial water saturation by a factor of roughly 10 %.

When all thick protective water lining pore walls are broken under case 1, the porous medium exhibits an I_{ow} of approximately zero. Since there are no longer water-wet pores, capillary pressure now drops rapidly from P_c^{max} to zero with little change in saturation upon imbibition. Upon drainage, capillary pressure still rises rapidly from P_c^{min} to zero with little change in saturation. These two results balance to give near neutral wettability. However, because the pore corners remain water-wet, the porous medium retains mixed-wettability character. Under case 2, strongly oil-wet behavior (I_{ow} near -1) results because the W/O emulsion films span all pores except the very smallest ones. These films all refill with oil while P_c is negative giving greater oil-wet character. Again, mixed-wettability is retained because the pore corners remain water-wet.

When P_c^{max} becomes infinite, S_{wc} approaches zero. All of the brine residing in pore corners is eliminated. In this instance all solid surfaces of the porous medium are oil-wet and an I_{ow} of -1 results.

The minimum imposed capillary pressure is set to $-P_c^{max}$ for all calculations. A less negative P_c^{min} does not force all of the water/oil interfaces of the bridging-oil lenses to touch. A distribution of lenses in which the interfaces have and have not touched arises in the mixed-oil-wet pores. In case 1 not all of the oil lenses become unstable. A mixture of broken and unbroken lenses at P_c^{min} gives capillary pressure curves which are a mixture of cases 1 and 2. The unbroken oil lenses refill in a manner analogous to the filling of the W/O emulsion films in case 2. In case 2, not all of the pores develop W/O emulsion films if P_c^{min} is made less negative. The capillary pressure curve is unaffected though. A more negative P_c^{min} also has no effect because there is very little additional oil to be recovered from the mixed-oil-wet pores in cases 1 and 2 .

Increasing the maximum in the solid/water/oil disjoining pressure curve (c.f. Fig. 3) adds stability to thick brine films coating pore walls. Thus, the P_c^* required (Eqn. (5)) to rupture thick films is increased. As Π^{max} is increased, the porous medium portrays more water-wetting character. In the limit of a very large disjoining pressure maximum (e.g., case 3), a completely water-wet porous medium results even with highly asphaltic oils present.

Pore shape also has significant effect on the results. For instance, in a concave pore, such as an eye-shaped pore (Fig. 14a) the thinnest brine films line the walls of the largest pores. A convex pore shape (c.f., Fig. 4) places the thinnest brine films in the largest pores. Hence with eye-shaped pores, the largest pores become mixed-oil-wet rather than the smallest oil-occupied pores. Remaining oil is still present as lenses or rivulets which bridge the corners

of pores. Since oil traps only in the smaller volume water-wet pores, residual oil saturation is now lower.

A triangular pore (Fig. 14b) allows all of the water films coating pore walls to break at the same capillary pressure. Results are similar to those when the imposed capillary pressure is very large. In this instance, P_c^* corresponds exactly to Π^{max} because the walls of triangular pores are of zero curvature. Residual oil saturation is drastically lower than in both the star and eye-shaped pores because all pores become mixed-oil-wet and undergo efficient drainage. As with both the star and eye-shaped pores, bridging-oil lenses are the source of remaining oil saturation. If bridging-oil lenses are unstable as in case 1, I_{ow} is approximately zero. For stable W/O emulsion films as in case 2, strongly oil-wet behavior (I_{ow} near -1) results, but these pores retain some mixed-wettability character because the corners of the pore are not oil-wet.

Morrow and Mason[29] find that in perfectly wetting triangular capillaries the amount of trapped oil is reduced as the triangle becomes more irregular. Recall that the area of the largest circle that can be inscribed in a pore (displayed in all pore shapes of Fig.14) determines the amount trapped oil. The more irregular a triangle, the smaller the possible inscribed circle relative to the total triangle area. Asymmetry in convex (Fig. 14c) or concave pore shapes also leads to less oil trapping and greater oil recovery.

The last pore shape considered is shown in Fig.14d. The walls of this star-shaped pore do not meet at a point. This type of shape arises if minerals deposit between grains[6]. The corners are rounded and do not retain significant amounts of brine at large imposed capillary pressures. Consequently, the entire pore wall becomes continuously oil-wet. If the imposed capillary pressure is again large, all pores are made oil-wet in this manner, the I_{ow} approaches -1 indicative of strongly oil-wet conditions.

The fifth model parameter is the pore-size distribution. By decreasing the ratio of large-sized pores to small-sized pores the amount of residual oil is reduced. Likewise, increasing the fraction of intermediate-sized mixed-oil-wet pores raises the amount of recoverable oil. Both of these changes shift I_{ow} toward more oil-wet conditions. When the smallest pores (representing micropores and pore throats) are trimmed from the distribution of pores sizes in Fig. 5 there are no longer small completely brine filled pores. Hence, S_{wc} falls close to zero. The shape of the capillary-pressure curves (i.e., Figs. 7 and 11) is not changed. They are merely shifted toward the left. Wettability indices are unaffected.

Our model allows exploration of not only mixed-wettability behavior, but a variety of wetting behaviors. Intermediate-wettability can be accommodated by altering the oil/water/solid disjoining pressure isotherm (c.f. Fig. 2) to represent surfaces of intermediate wettability. In fact, a surface with virtually any type of wettability can be modeled by using the appropriate disjoining pressure isotherm. Also, we are not limited to surfaces of uniform wettability. One portion of a surface may be represented by a disjoining pressure isotherm for water-wetting minerals and another for oil-wetting minerals. Furthermore, our picture explains mechanistically how surfaces may remain water-wet even when highly asphaltic oil is present.

Conclusions

Currently most models of flow in porous media are based on interconnected networks of pores whose typical shapes are either cylinders or unspecified. Although network models are very successful in explaining concepts such as relative permeability and trapping, they do not address the important issues of wettability and wettability alteration. At a fundamental level, nonaxysymmetric pore shapes and thin films are necessary to understand wettability.

We find that a delicate interplay between pore shape and thin-film chemistry and physics can predict mixed-wettability in porous rocks. In a distribution of star-shaped pores, the largest star-shaped pores are prevented from becoming mixed-oil-wet because their pore walls are protected by thick continuous water films. These films prohibit asphaltene adsorption and subsequent alteration in the wettability state of the pore surface. Conversely, ultrathin, molecular films form on the walls of intermediate-sized star-shaped pores during pristine drainage. These films permit irreversible asphaltene adsorption, and subsequently these pores become mixed-oil-wet. The smallest pores which are never entered by oil remain water-wet.

Our proposed suite of pore-level events correctly describes the essential observations associated with mixed-wettability reservoir rocks. Capillary pressure curves mimic those generated experimentally in the laboratory. Foremost, a significant reduction, compared to water-wet rock, in residual oil saturation is predicted. The correct trends of wettability index are found. Lower initial brine saturations lead to greater oil-wettability.

Remaining oil saturation, the long period of oil production, and high-efficiency waterfloods of mixed-wettability systems are attributed to the formation of thick oil lenses or rivulets which span the corners of pores in addition to oil films adhering to pore walls. Oil drainage is consequently very slow. With star-shaped pores these lenses or rivulets reside in pores of intermediate size. The notion of contact angle-pinning allows development of the bridging oil lenses.

Because the largest pores remain water-wet, oil snaps off and is trapped in a manner identical to the creation residual oil in completely water-wetting porous media. Irreducible snapped-off water is also formed because brine is trapped in mixed-oil-wet pores in a fashion similar to the creation of residual oil in water-wet porous media. In contrast to water-wet systems, connate and irreducible water saturation are shown to be quite different in mixed-wettability systems. Since wettability states undergo change at or near S_{wc}, there is a corresponding change in pore-level mechanisms for mixed-wettability systems. Irreducible water, consistent with experimental observations, is predicted to be greater for mixed-

wettability systems than for water-wetting systems due to the formation of discontinuous trapped water.

Nomenclature

a= radius of circle which can be inscribed in pore, m
A_i = cross sectional area, m^2
d_i= bead diameter, m
h = equilibrium film thickness, m
h_i = equilibrium film thickness overlay a bead of diameter d_i, m
h_p= range of film thickness where disjoining pressure is relevant, m
I_{ow}= Amott-Harvey wettability index
P_c = capillary pressure, difference in oil and water phase pressure, N/m^2
P_{nw} = nonwetting phase pressure, N/m^2
P_w = wetting phase pressure, N/m^2
r_1, r_2 = principal radii of curvature, m
S_i = phase saturation, ratio of the area occupied by a phase to total area of the system

Subscripts and Superscripts

* = critical value for thick film rupture
e = entry for a particular size pore
max = maximum
m = mean
o = oil
or = residual oil
t = total
w = water
wc = connate water
wirr = irreducible water

Greek letters

Π = disjoining pressure, Pa
σ = interfacial tension, N/m
θ = equilibrium contact angle measured through the aqueous phase
ΔS_{os}=saturation change during secondary drainage
ΔS_{ws}=saturation change during spontaneous imbibition
ΔS_{wt}=overall saturation change during imbibition
ξ = dummy variable of integration, m

Acknowledgement

This work was supported by the U.S. Department of Energy under contract No. DC03-76SF00098 to the Lawrence Berkeley Laboratory of the University of California.

References

1. Morrow, N. R., H. T. Lim, and J. S. Ward: "Effect of Crude-Oil Induced Wettability Changes on Oil Recovery," SPEFE (Feb. 1986) 89-103.

2. Jadhunandan, P. P. and N. R. Morrow: "Effect of Wettability on Waterflood Recovery for Crude-Oil/Brine/Rock Systems, SPE 22597, presented at 1991 SPE Annual Tech. Conf., Dallas, TX.

3. Craig, F. F. Jr.: The Reservoir Engineering Aspects of Waterflooding, Society of Petroleum Engineers of AIME, New York (1971) 12-19 .

4. Cueic, L. E.: "Evaluation of Reservoir Wettability and Its Effect on Oil Recovery," in Interfacial Phenomena in Petroleum Recovery, N. R. Morrow ed., Marcel Dekker Inc, New York (1991) Ch.9 319-373.

5. Morrow, N. R.: "Introduction to Interfacial Phenomena in Oil Recovery," in Interfacial Phenomena in Petroleum Recovery, N. R. Morrow ed., Marcel Dekker Inc, New York (1991) Ch. 1 1-22.

6. Salathiel, R. A.: "Oil Recovery by Surface Film Drainage in Mixed-Wettability Rocks," JPT (Oct. 1973)1216-1224.

7. Fassi-Fihri, O., M. Robin, and E. Rosenberg: "Wettability Studies at the Pore Level: A New Approach by the Use of Cryo-Scanning Electron Microscopy," SPE 22596, presented at 1991 SPE Annual Tech. Conf., Dallas, TX.

8. Derjaguin, B. V., Z. M. Zorin, N. V. Churaev, and V. A. Shishin: "Examination of Thin Layers on Various Solid Substrates," in Wetting, Spreading and Adhesion, J. F. Padday ed., Academic Press, London (1978) Ch. 9 201-212.

9. Derjaguin, B. V. and E. V. Obukhov: "Anomalien dünner Flüssigkeitsschichten III," Acta Physicochim. URSS (1936) 5(1) 1-22.

10. Derjaguin, B. V. and M. M. Kussakov: "Anomalous Properties of Thin Polymolecular Films V.," Acta Physicochim. URSS (1939)10(1) 25-44.

11. Derjaguin, B. V. and M. M. Kussakov: "Anomalous Properties of Thin Polymolecular Films V.," Acta Physicochim. URSS (1939) 10(2) 153-174.

12. Derjaguin, B. V., N. V. Churaev, and V. M. Muller: Surface Forces, Consultants Bureau, New York (1987) 25-52,327-367.

13. Chambers, K. T. and C. J. Radke:"Capillary Phenomena in Foam Flow Through Porous Media," in Interfacial Phenomena in Petroleum Recovery, N. R. Morrow ed., Marcel Dekker Inc, New York (1991) Ch.1 191-255.

14. Melrose, J. C.: "Interpretation of Mixed Wettability States in Reservoir Rocks," SPE 10971, presented at 1982 SPE Fall Tech. Conf. , New Orleans, LA.

15. Callaghan, I. C. and K. W. Baldry: "The Thickness of Aqueous Wetting Films on Silica," in Wetting Spreading and Adhesion, J. F. Padday ed., Academic Press, London (1978) Ch.7 161-181.

16. Hall, A. C., S. H. Collins, and J. C. Melrose: "Stability of Aqueous Wetting Films in Athabasca Tar Sands," SPEJ (Apr. 1983) 249-258.

17. Hirasaki G. J.: "Wettability: Fundamentals and Surface Forces," SPEFE (Jun. 1991) 217-226.

18. Morrow, N. R.: "Wettability and Its Effect on Oil Recovery," JPT (Dec. 1990)1476-1484.

19. Buckley, J. S., K. Takamura, and N. R. Morrow: "Influence of Electrical Surface Charges on the Wetting Properties of Crude Oil," SPERE (Aug. 1989) 332-340.

20. Buckley, J. S. and N. R. Morrow: "Characterization of Crude-Oil Wetting Behavior by Adhesion Tests," SPE 20263 presented at the 1990 SPE/DOE Symposium on Enhanced Oil Recovery, Tulsa, OK.

21. Wong, H., S. Morris, and C. J. Radke: "Three Dimensional Menisci in Polygonal Capillaries," J. Coll. Inter. Sci (1992) 148(2) 317-336.

22. Dubey, S. T. and M. H. Waxman: "Asphaltene Adsorption and Desorption From Mineral Surfaces," SPERE (Aug. 1991) 389-395.

23. Chung, F., Sarathi, P., and Jones, R.: "Modeling of Asphaltene and Wax Precipitation," NIPER-498,1991 DOE Topical Report, Bartlesville, OK .

24. Clementz, D. M.: "Interaction of Petroleum Heavy Ends with Montmorillonite," Clays and Clay Min. (1976) 24, 312-319 .

25. Clementz, D. M.: "Alteration of Rock Properties by Adsorption of Petroleum Heavy Ends: Implications for Enhanced Oil Recovery," SPE 10683 presented at 1982 SPE/DOE Joint Symposium on Enhanced Oil Recovery, Tulsa, OK.

26. Hirasaki, G. J., J. A. Rohan, S. T. Dubey: "Wettability Evaluation During Restored-State Core Analysis," SPE 20506, presented at 1990 SPE Annual Tech. Conf., New Orleans, LA.

27. Wardlaw, N. C., Y. Li ., and D. Forbes: "Pore-Throat Size Correlation from Capillary Pressure Curves," Transport in Porous Media (1987) 2 597-614.

28. Mayer, R. P. and R. A. Stowe: "Mercury Porosimetry--Breakthrough Pressure for Penetration between Packed Spheres," J. Coll. Interf. Sci. (1965) 20 893-911.

29. Morrow, N. R. and G. Mason: "Capillary Behavior of a Perfectly Wetting Liquid in Irregular Triangular Tubes," J. Coll. Interf. Sci (1991) 141(1) 262-274.

30. Kovscek, A. R., PhD Dissertation: University of California, Berkeley (1992) in progress.

31. Ransohoff, T. C., P. A. Gauglitz, and C. J. Radke: "Snap-Off of Gas Bubbles in Smoothly Constricted Noncircular Capillaries," AIChE Journal (1987) 33(5) 753-765 .

32. Roof, J. G.: "Snap-Off of Oil Droplets in Water-Wet Pores," SPEJ (Mar. 1970)85-90.

33. Mohanty, K. K. and A. E. Miller: "Factors Influencing Relative Permeability of a Mixed-Wet Reservoir Rock," SPEFE (Sep. 1991) 349-358.

34. Amott, E.: "Observations Relating to the Wettability of Porous Rock," Trans AIME (1959) 216, 156-162.

35. Mohanty, K. K., H. T. Davis, and L. E. Scriven: "Physics of Oil Entrapment in Water-Wet Rock," SPERE (Feb.1987) 113-128.

Table 1: Amott-Harvey Indices and Residual Oil Saturation for Water-Wet and Mixed-Wet Porous Media

case	$\frac{a_m \Pi^{max}}{\sigma}$	I_{ow}	S_{or}
1: unstable lenses	18	0.36	0.35
2: stable W/O emulsion films	18	-0.18	0.35
3: water-wet	180	1.0	0.54

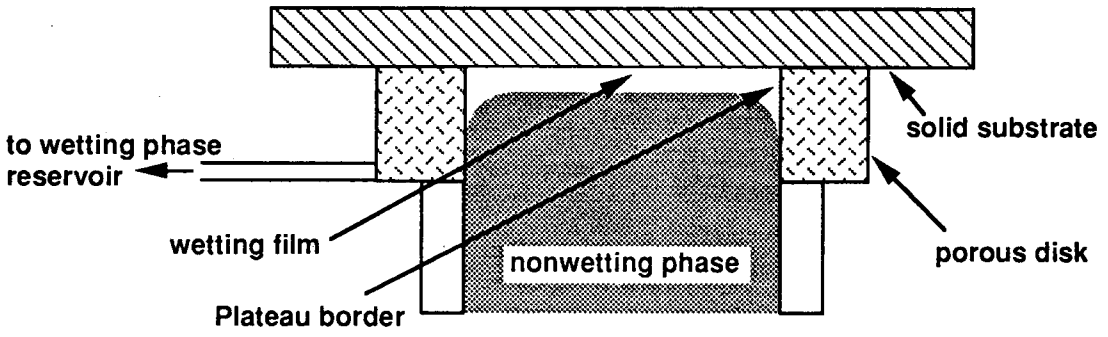

Figure 1: Schematic diagram of of an apparatus for measuring thin-film forces in solid/liquid systems (after ref. 8)

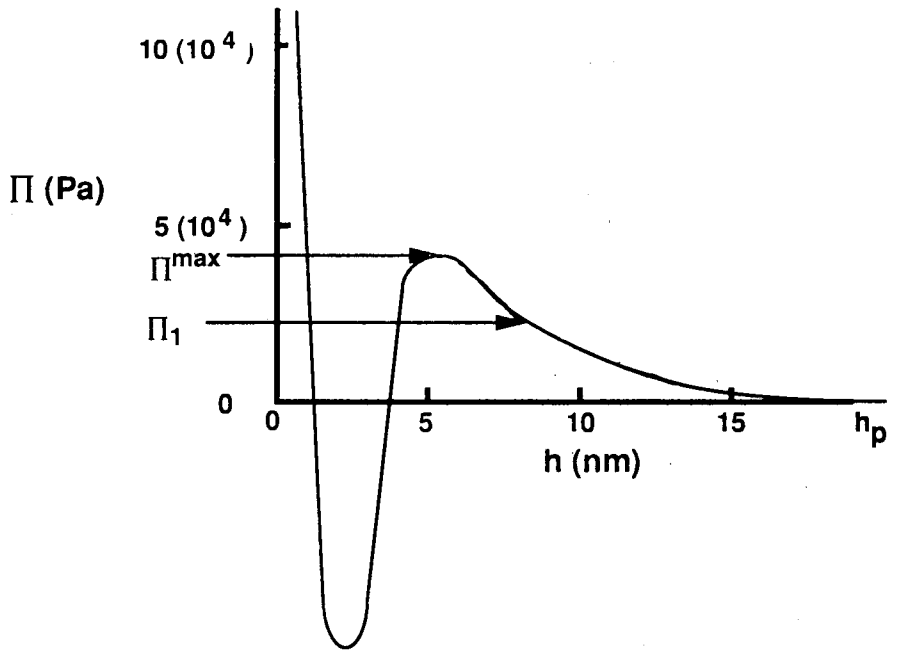

Figure 2 : Schematic disjoining pressure isotherm for wetting films on solids

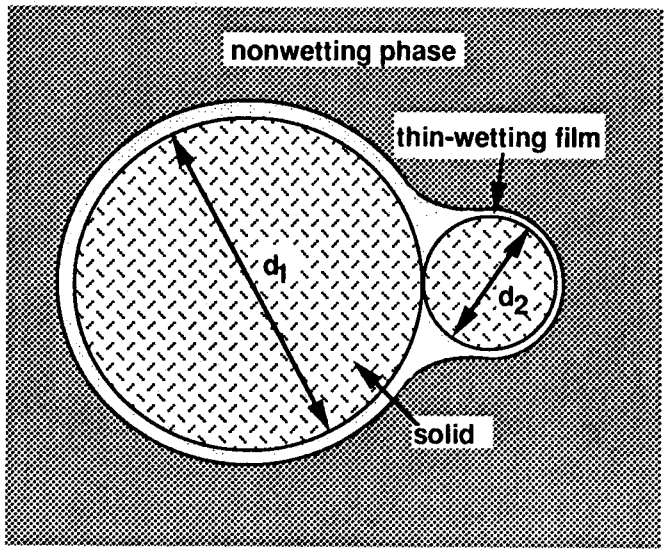

Figure 3: Wetting films covering solid spheres.

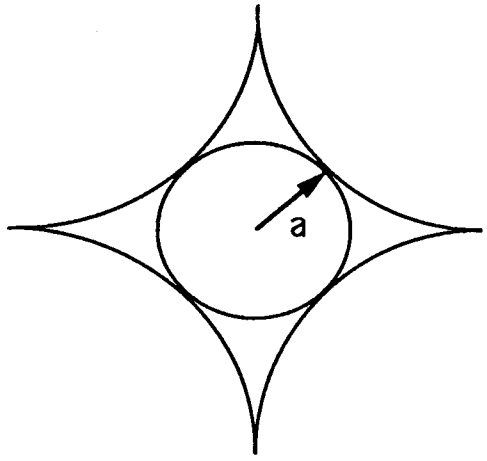

Figure 4: Cross section of a star-shaped translationally invariant pore.

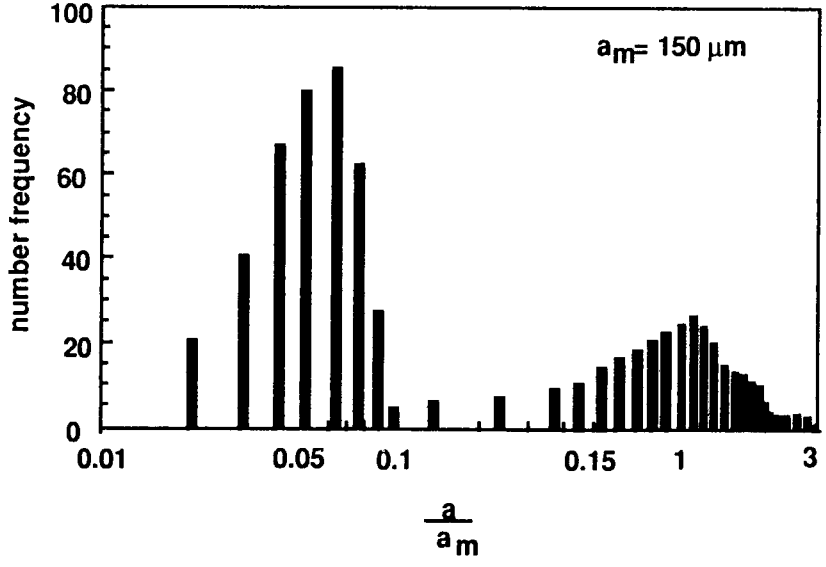

Figure 5: Discrete size distribution of star-shaped pores.

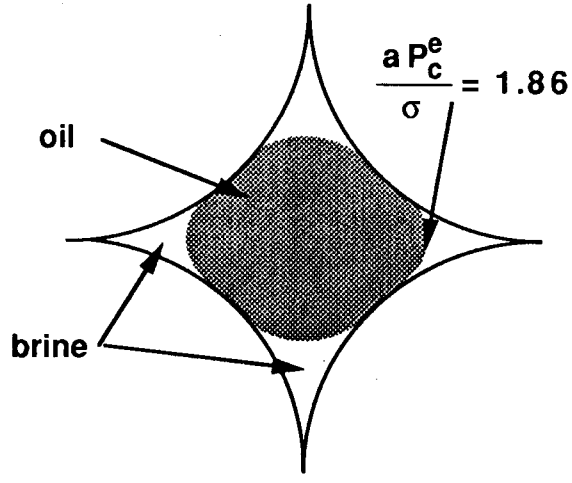

Figure 6: Water-wet pore just after oil entry

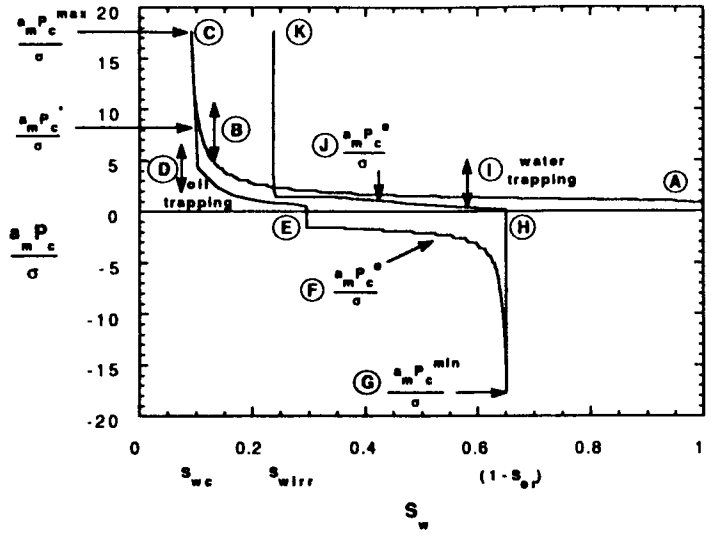

Figure 7: Capillary pressure versus aqueous phase saturation, case 1 unstable lenses.

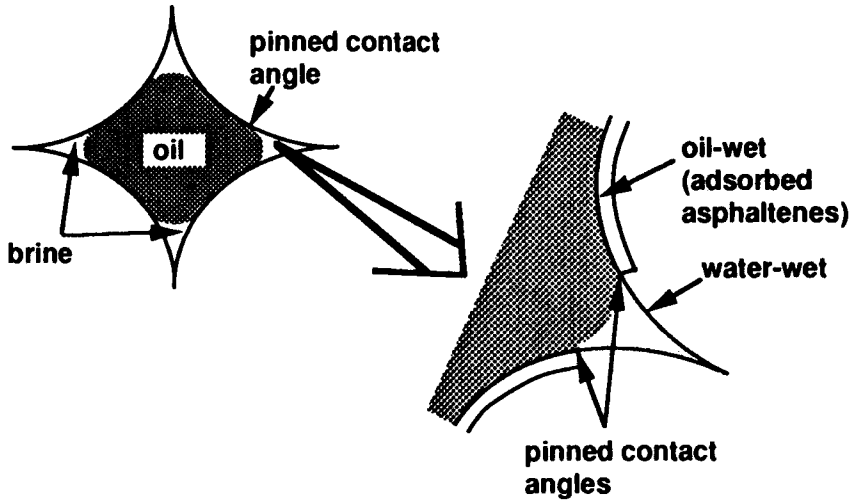

Figure 8: Schematic of a mixed-oil-wet pore illustrating the location of asphaltene deposition and the coexistence of oil-wet and water-wet regions within a single pore.

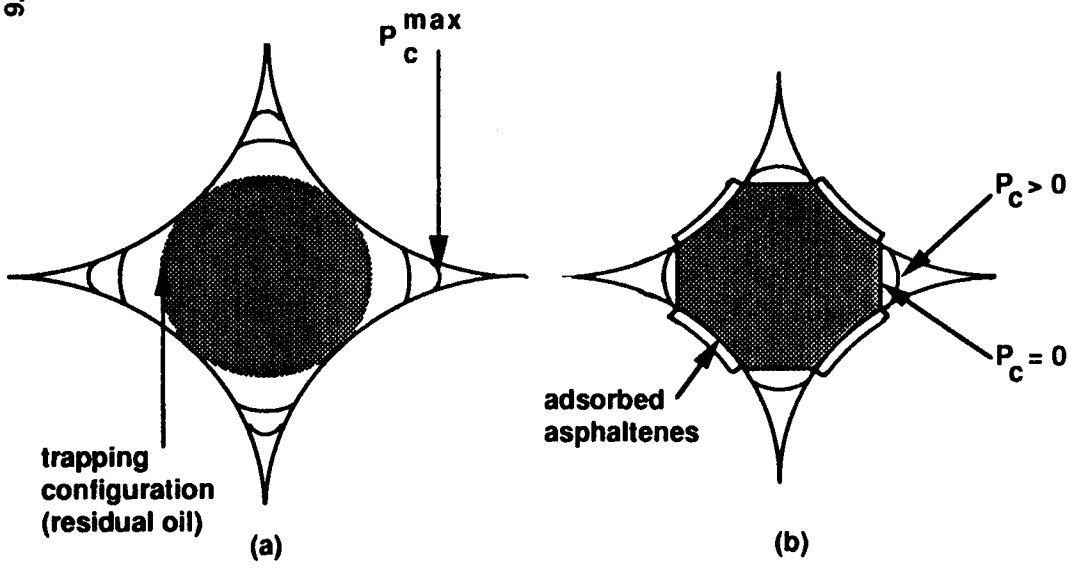

Figure 9: Imbibition processes in water-wet (a) and mixed-oil-wet (b) pores during forced imbibition.

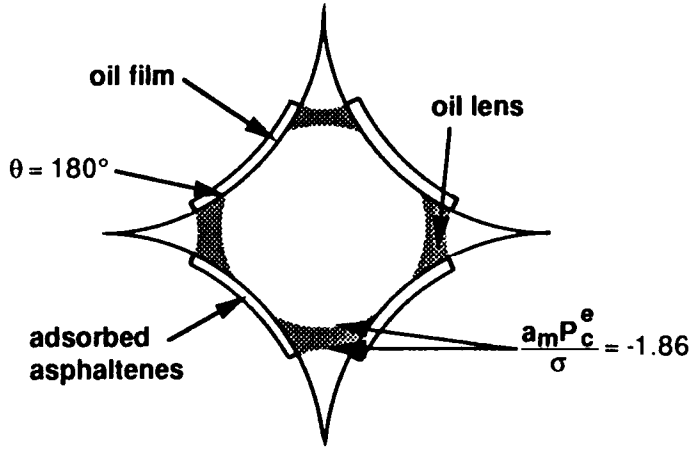

Figure 10: Phase configurations just after brine entry into a mixed-oil-wet during forced imbibition

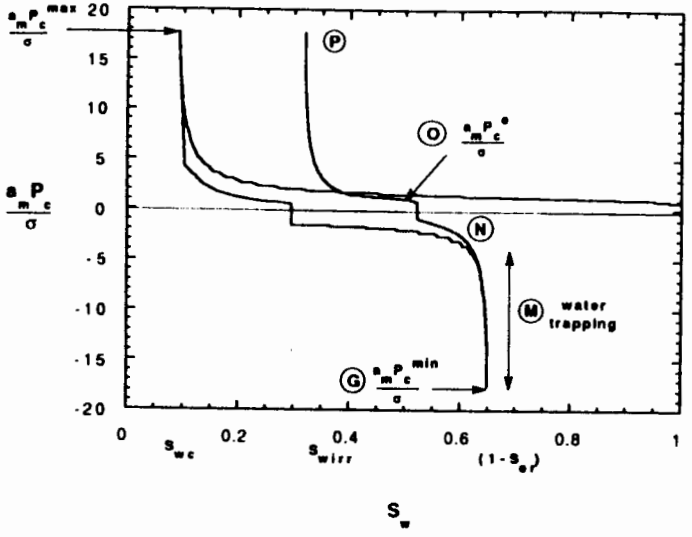

Figure 11: Capillary pressure versus aqueous phase saturation, case 2 stable W/O emulsion films.

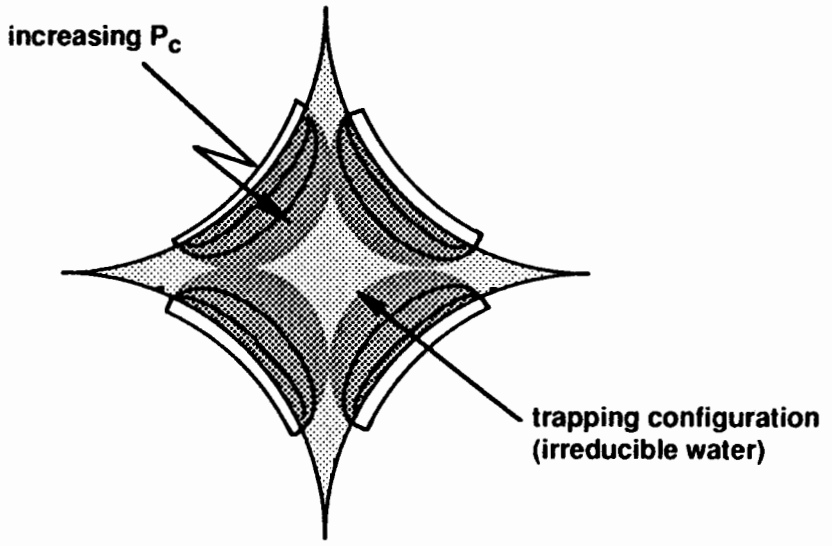

Figure 12: Secondary drainage in mixed-oil-wet pores, case 1 unstable lenses.

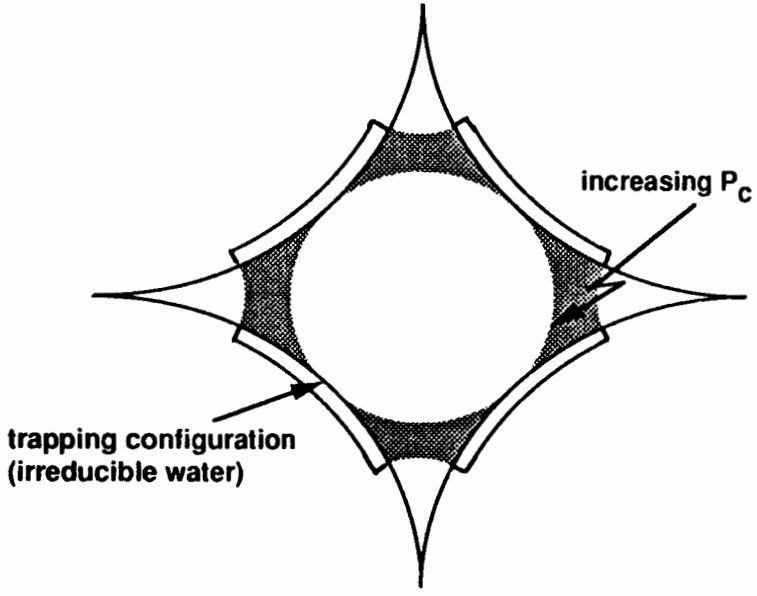

Figure 13: Secondary drainage in mixed-oil-wet pores, case 2 stable W/O emulsion films.

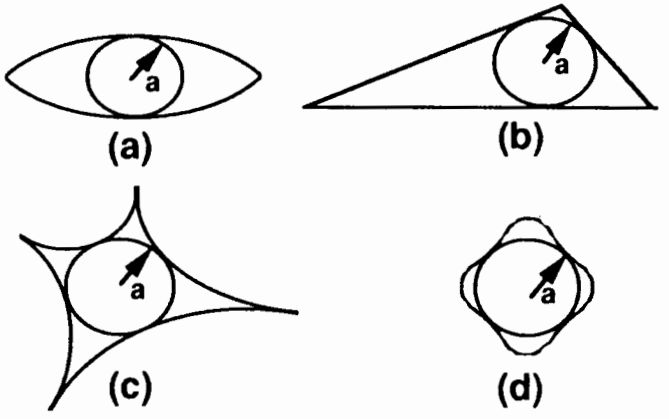

Figure 14: Alternative cross-sectional pore shapes (a) eye-shaped (b) irregular-triangle (c) irregular-star (d) star-shaped with mineral deposits in pore corners.